Supplemental materials for "Controlling mechanisms in directional growth of aggregated archaeal cells"

Viktor Milkevych, Damien J. Batstone

1. Details in fine structure of *Methanosarcina* cell wall

The cell wall consists of three major components: cytoplasmic membrane, surface layer proteins (S-layer) and heteropolysaccharide layer (matrix) [1]. The cytoplasmic membrane appears in bilayer structure of hydroxylated diether lipids (3-hydroxyarchaeols) [2, 3], with a thickness of bilayer 4.5nm [1]. The S-layer is the outmost boundary of the cell envelop and can be considered as a protective, porous barrier [4], with an average thickness of the layer $10-12\text{nm}$ [5, 6]. This structure can be represented in a series of hexagonal tiles where the each particular tile consists of six complete C-terminal dimers and halves of an additional six C-terminal dimers [4]. Each particular tile connects with six surrounding tiles through the network of intermolecular interactions. These connections generate the extensive pore network with three different pore types with the pore size range $8-13\text{Å}$ [4]. The third component, the heteropolysaccharide matrix, has a thickness of $20-200\text{nm}$ and is composed of fibrillar polymer methanochondroitin, which possess a molecular mass of about 10kDa [7]. The matrix appears as loosely packed fibrils initially polymerized parallel to the S-layer [8]. The range of matrix thickness values can be reduced to $60-100\text{nm}$ by excluding from consideration the degenerate methanohondroitin, where depolymerization leads to a decrease in matrix density, external spreading of fibrils and, finally, further depletion of the matrix thickness [5, 6]. Methanochondroitin consists of trisaccharide repeating unit of two N-acetylgalactosamines (GalNAc) and one glucuronic acid (GlcA). It is similar to eukaryotic chondroitin with respect to overall composition and structure [9]. Eukaryotic chondroitin is in a semiflexible coil conformation of twofold helix polymer, with an intrinsic persistence length of $45-55\text{Å}$ [10-12]. Taking into account the similarities between methanochondroitin and chondroitin molecules both polymers should have similar conformational behavior.

2. Derivation the growth eigenstrain rate equation

The cell Θ in reference configuration $\bar{\xi}$ (see Fig.3 in the main text and section 3 in current Supplementary materials) has a density $\rho_0 = \rho \cdot \det(\boldsymbol{F})$, where ρ is the density in actual configuration, with $\det(\boldsymbol{F}) > 0$. According to [13-15] the rate of ρ_0 in reference configuration proportional to $\boldsymbol{E}_0 : \dot{\boldsymbol{G}}\boldsymbol{G}^{-1}$: $\dot{\rho}_0 \sim \rho_0 \boldsymbol{E}_0 : \dot{\boldsymbol{G}}\boldsymbol{G}^{-1}$, where $\boldsymbol{E}_0$ is the tensor that describe the absorption rate anisotropy; the upper dot corresponds to the material time derivative. Addition of the sink term to this equation results in the following:

$$\dot{\rho}_0 = \rho_0 \boldsymbol{E}_0 : \dot{\boldsymbol{G}}\boldsymbol{G}^{-1} - \rho_0 \boldsymbol{E}_{\delta} : \boldsymbol{I}\,, \quad \text{(S1)}$$

where $\boldsymbol{E}_{\delta}$ is the tensor that describe the desorption rate. The conservation of mass for methanochondroitin matrix can then be written as:

$$\rho_0 \dot{\phi} = \mathrm{div}_{\bar{\xi}} \left(\phi \rho_0 \boldsymbol{v}\right) + \rho_0 \boldsymbol{E}_{\boldsymbol{p}} : \dot{\boldsymbol{G}}\boldsymbol{G}^{-1} - \rho_0 \boldsymbol{E}_{\boldsymbol{d}} : \boldsymbol{I}\,, \quad \text{(S2)}$$

where ϕ is cell wall polymer concentration; $\boldsymbol{v}$ is the flux rate of polymer filaments through the surface Ω_{free} (methanochondroitin mechanical detachment towards the extracellular media as well as surface depolymerization), $\boldsymbol{E}_{\boldsymbol{p}}$ is the tensor that describe the anisotropy in monosaccharaides polymerization rate inside the cell wall and $\boldsymbol{E}_{\boldsymbol{d}}$ is the tensor that describe the depolymerization rate of methanochondroitin inside the cell wall.

The cell wall material (see the section 2.2.1 in the main text for more details) can be characterized by chemical potential μ_{conf} which is a function of polymer concentration and confinement strength characterized by confinement size d: $\mu_{\text{conf}} = \mu_{\text{conf}}\left(\phi, d\right)$. μ_{conf} can be represented as an additive decomposition [16]:

$$\mu_{\text{conf}} = \mu_{\text{conf}}\left(\phi\right) + \mu_{\text{conf}}\left(d\right), \quad \text{(S3)}$$

where $\mu_{\text{conf}}\left(\phi\right)$ accounts for the concentration dependence of unconfined methanochondroitin solution and $\mu_{\text{conf}}\left(d\right)$ accounts for the confinement dependence of isolated methanochondroitin filament. The relation between confining tube diameter d and the free energy of such confinement is given as $\beta\Psi_{\text{conf}} = \mathrm{cL}\lambda^{-1}$ [17-19], where β is the inverse of the thermal energy; c is dimensionless prefactor; L is the length of the tube; λ is a deflection length, $\lambda = l_p^{1/3} d^{2/3}$; l_p is a persistence length of the polymer chain. Instead of d, another characteristic variable – the inverse of deflection length $\lambda_* = \lambda^{-1}$ may be used. During cell wall growth due to different $\boldsymbol{E}_{\boldsymbol{p}}$ and $\boldsymbol{E}_{\boldsymbol{d}}$ one can observe anisotropy in polymerization-depolymerization processes and hence in local density change. Such local density changes exert changes in polymer confinement and hence the changes in λ_* such that the higher polymerization rate inside the cell wall leads to a decrease in confined tube diameter (and increase of λ_*). In this context, the rate of λ_* should be proportional to $\rho_0 \boldsymbol{E}_{\boldsymbol{p}} : \dot{\boldsymbol{G}}\boldsymbol{G}^{-1}$ and $-\rho_0 \boldsymbol{E}_{\boldsymbol{d}} : \boldsymbol{I}$. In general, one can assume that the rate of λ_* should follow the same dynamics as $\rho_0 \phi$, so the following relation can be considered:

$$\dot{\lambda}_* \simeq \gamma \dot{\phi}\,, \quad \text{(S4)}$$

where γ is some function which provide correct conformity between the phase space of polymer's concentration and phase space of polymer's confinement characteristic value.
The balance of internal energy $\mathcal{E}$ has the following form:

$$\rho_0 \dot{\mathcal{E}} = T\dot{S} - \dot{R} + \mathrm{div}_{\bar{\xi}}\left(\mu_{\mathrm{conf}} \cdot \boldsymbol{m}\right), \quad \text{(S5)}$$

where T is a temperature; S is entropy; $\boldsymbol{m} = \phi\rho_0\boldsymbol{v}$. By taking into account the expression for the free energy $\Psi = \mathcal{E} - TS$, the free energy of confined elastic shell can be represented as:

$$\rho_0 \dot{\Psi} = -\dot{R} - S\dot{T} + \mathrm{div}_{\bar{\xi}}\left(\mu_{\mathrm{conf}} \cdot \boldsymbol{m}\right). \quad \text{(S6)}$$

Following the general idea about the representation of Ψ as it was introduced in [20], the free energy of confined elastic shell is specified as $\Psi = \Psi\left(\boldsymbol{F_e},\ \lambda_*,\ \phi,\ T\right)$. The rate of Ψ now reads:

$$\dot{\Psi} = \frac{\partial \Psi}{\partial \boldsymbol{F_e}} : \dot{\boldsymbol{F}}_{\boldsymbol{e}} + \frac{\partial \Psi}{\partial \lambda_*}\dot{\lambda}_* + \frac{\partial \Psi}{\partial \phi}\dot{\phi} + \frac{\partial \Psi}{\partial T}\dot{T}. \quad \text{(S7)}$$

Next, by recalling equations (6) and (7) (in the main text), (S1), (S2), (S4) and (S7) from (S6) one can obtain, after some transformation and neglecting the thermal terms, the dissipation inequality:

$$\begin{aligned}&\left[\varphi \boldsymbol{F}_{\boldsymbol{e}}^{\boldsymbol{T}}\boldsymbol{P}\boldsymbol{G}^{\boldsymbol{T}} - \rho\Psi\boldsymbol{E}_0 - \rho\left(\partial_\phi\Psi - \gamma\partial_{\lambda_*}\Psi\right)\boldsymbol{E_p}\right] : \dot{\boldsymbol{G}}\boldsymbol{G}^{-1} + \left[\mu_{\mathrm{conf}} - \partial_\phi\Psi - \gamma\partial_{\lambda_*}\Psi\right]\mathrm{div}_{\bar{\xi}}\left(\boldsymbol{m}\right) + \\ &\left[\varphi\boldsymbol{P}\boldsymbol{G}^{\boldsymbol{T}} - \rho\partial_{\boldsymbol{F_e}}\Psi + \left(1-\varphi\right)\mathbf{P}\right] : \dot{\boldsymbol{F}} + \left[\rho\left(\partial_\phi\Psi - \gamma\partial_{\lambda_*}\Psi\right)\boldsymbol{E_d} + \rho\Psi\boldsymbol{E_\delta}\right] : \boldsymbol{I} + \boldsymbol{m}\cdot\mathrm{grad}\left(\mu_{\mathrm{conf}}\right) \geq 0\end{aligned} \quad \text{(S8)}$$

Following the same way as it is described in details in [13, 14] (S8) can be reformulated, which now takes the form:

$$\left[\varphi \boldsymbol{F}_{\boldsymbol{e}}^{\boldsymbol{T}}\boldsymbol{P}\boldsymbol{G}^{\boldsymbol{T}} - \rho\Psi\boldsymbol{E}_0 - \rho\mu_{\mathrm{conf}}\left(\phi,\lambda_*\right)\boldsymbol{E_p}\right] : \dot{\boldsymbol{G}}\boldsymbol{G}^{-1} \geq 0, \quad \text{(S9)}$$

$$\boldsymbol{m}\cdot\mathrm{grad}\left(\mu_{\mathrm{conf}}\right) \geq 0,$$

where

$$\mu_{\mathrm{conf}}\left(\phi,\lambda_*\right) = \partial_\phi\Psi + \gamma\partial_{\lambda_*}\Psi \equiv \mu_{\mathrm{conf}}\left(\phi\right) + \mu_{\mathrm{conf}}\left(\lambda_*\right), \quad \text{(S10)}$$

which follows from (S8). The dissipation inequality (S9) is similar to that reported in [13-15] but the differences, some of which are: a) the function φ that defines the partial contribution of mechanical work to the cell wall growth and b) different definition for chemical potential μ_{conf}, which is derived here in form (S10).

According to [13-15], dissipation inequality like (S9) can be always satisfied if we apply the following condition:

$$\varphi\boldsymbol{F}^{\boldsymbol{T}}\boldsymbol{P} - \rho\Psi\boldsymbol{E}_0 - \rho\mu_{\mathrm{conf}}\left(\phi,\lambda_*\right)\boldsymbol{E_p} = \chi^{-1}\left(\phi\right)\dot{\boldsymbol{g}}, \quad \text{(S11)}$$

where $\chi(\phi)$ is a scalar function of ϕ, $\dot{\boldsymbol{g}}$ is the growth eigenstrain rate.

3. Geometry of aggregated cell

The archaeal cell can be represented as a body Θ embedded in the three dimensional space $\mathbb{R}^3$ with intrinsic properties determined by the above. The model of $\Theta \in \mathbb{R}^3$ is represented in a curvilinear coordinate system ξ^α $(\alpha = 1,2)$ (see Fig. 3 in the main text). The cell wall is represented by a smooth surface $\Omega_0 \in \mathbb{R}^2$ where the each point has a neighborhood that is regularly parameterized by ξ^α, with ξ^α being two-dimensional Gaussian coordinates. Applying 3D space parametrization in the neighborhood of Ω_0 results in the following equation for a radius vector for any point in Θ [21, 22]: $\boldsymbol{R}(\xi^\alpha, \varsigma) = \boldsymbol{r}(\xi^\alpha) + \varsigma \boldsymbol{n}(\xi^\alpha)$, where $\boldsymbol{r}(\xi^\alpha)$ is the parametrization of Ω_0 with unit-normal field $\boldsymbol{n}(\xi^\alpha)$, ς is the coordinate counted along the direction perpendicular to Ω_0, $\varsigma \in [-h/2, h/2]$, h is cell wall thickness. The initial position of Ω_0 opted relative to the top and bottom surfaces of the cell wall $\Omega_{\text{top, bot}}$, the radius vectors of which defined as $\boldsymbol{R}_{\text{top, bot}} = \boldsymbol{r} \pm \boldsymbol{n}h/2$. The tangential vectors of Ω_0 which constitute the co-variant and contravariant bases on Ω_0 are given by [21-23] $\boldsymbol{r}_\alpha = \partial \boldsymbol{r} / \partial \xi^\alpha$, $\boldsymbol{r}_\alpha \cdot \boldsymbol{r}^\beta = \delta_\alpha^\beta$, $(\alpha, \beta = 1,2)$, where δ_α^β is the Kronecker symbol. Note, that the following condition is satisfied $\boldsymbol{r}_1 \times \boldsymbol{r}_2 \neq 0$. The unit vector normal to Ω_0 defined $\boldsymbol{r}_3 = \boldsymbol{r}_1 \times \boldsymbol{r}_2 / |\boldsymbol{r}_1 \times \boldsymbol{r}_2|$. The metric tensor has a form $g_{\alpha\beta} = \boldsymbol{r}_\alpha \cdot \boldsymbol{r}_\beta$, $g^{\alpha\beta} = \boldsymbol{r}^\alpha \cdot \boldsymbol{r}^\beta$, $(\alpha, \beta = 1,2)$. The curvature tensor $\boldsymbol{k}$ of Ω_0 can be expressed through the following equation $d\boldsymbol{n} = -\boldsymbol{k} d\boldsymbol{r}$, where $d\boldsymbol{r} = \boldsymbol{r}_\alpha d\xi^\alpha$, $d\boldsymbol{n} = \boldsymbol{n}_\alpha d\xi^\alpha$.

Another curvilinear coordinate system $\bar{\xi}^\alpha$ $(\alpha = 1,2)$ can also be considered, which characterizes the geometry of Θ in the initial, reference, configuration (before any deformation). All necessary geometric relations based on $\bar{\xi}^\alpha$ can be constructed in the same way as it was done above.

Consider also the ratio h/b at any point $p \in \Omega_0$, here b is local radius of curvature. Taking into account the observation data [24-26] for *h* and *b*, calculated maximum average values of 0.053 have been observed for this relation. Because of this h can be considered as sufficiently small against other length scales of the cell, so it is reasonable to represent the cell as a confined thin elastic shell.

4. Representative conformation of confined shell

The natural processes of enzymatic, diffusion and protein oscillations of the cell [27-30] are the foundation of more complex cell processes that can be effectively represented by a stochastic

approximation (refer to [31, 32] as for particular examples). Within such an approach, consider the cell state functional $U^*[\boldsymbol{R}]$ of the cell geometry $\boldsymbol{R}(\xi^\alpha, \varsigma)$, that itself depends on cell wall growth anisotropy, placement and rotation of division plane, changes in confinement state. Here we can apply the statistical mechanics approach and assume a finite number of theoretically possible states (with a proper values of $U^*[\boldsymbol{R}]$) which the cell can occupy. It is convenient to consider some distribution function describing the probability density of observing the cell Θ_i in configuration $\boldsymbol{R}(\xi^\alpha, \varsigma)|_t^i$ in the aggregate at the time t. In this context, the representative configuration is that more likely observed in aggregate at certain moment of time, in other words, the representative configuration $\boldsymbol{R}|_t^{\text{rep}}$ corresponds to the cell state U^{rep} with a highest probability value.

Since the model for the cell has been determined as above, the configuration of the confined cell by means of conformation of surface Ω_0 is specified by $\boldsymbol{r}(\xi^\alpha)$. In this context, $U[\boldsymbol{r}]$ defines the mapping between the space conformation $\boldsymbol{r}(\xi^\alpha)$ of surface Ω_0 and potential energy U of the cell. The well-known conformation partition function (for particular moment of time) for this case can be written: $Z = \int \mathrm{D}\boldsymbol{r} \exp(-\beta U[\boldsymbol{r}])$, where $\int \mathrm{D}\boldsymbol{r}$ indicates a functional integral over all possible space conformations $\boldsymbol{r}(\xi^\alpha)$ that describe the shape of the cell, β is inverse of the thermal energy. For the particular conformation $\boldsymbol{r}(\xi^\alpha)|^m$ the following expression can be introduced: $Z_m = \exp(-\beta U[\boldsymbol{r}|^m])$. Thereby, the joint probability density of observing a cell in configuration $\boldsymbol{r}(\xi^\alpha)|^m$ is the distribution: $P_m = Z_m / Z$, normalized as $\int \mathrm{D}\boldsymbol{r}\, P[\boldsymbol{r}] = 1$. The representative conformation of shell (or configuration of cell) at the discrete time interval t_i may now be determined as $\boldsymbol{r}|_{t_i}^{\text{rep}} = \{\boldsymbol{r}(\xi^\alpha)|^m : \max\{P(\boldsymbol{r})\}|_{t_i}\}$.

5. Principal directions of growth and growth anisotropy

In order to validate the developed model, and overall theoretical approach to study the growth of aggregated cells, we use the reported elsewhere observations (see the introduction section for cited references) regarding division plane orientation and their alteration for both archaea and bacteria. Since our study, in general, and the models output, in particular, is focusing only on principal directions of cell wall growth but not on division plane positioning, we predict such principal growth directions based on reported information for division planes orientation and use this information for model validation. Such prediction is straightforward, according to reported studies [33-37], division plane positioned orthogonally to the longest axes of the cell and hence to the principal direction of cell wall growth (Fig. S2 (a)).

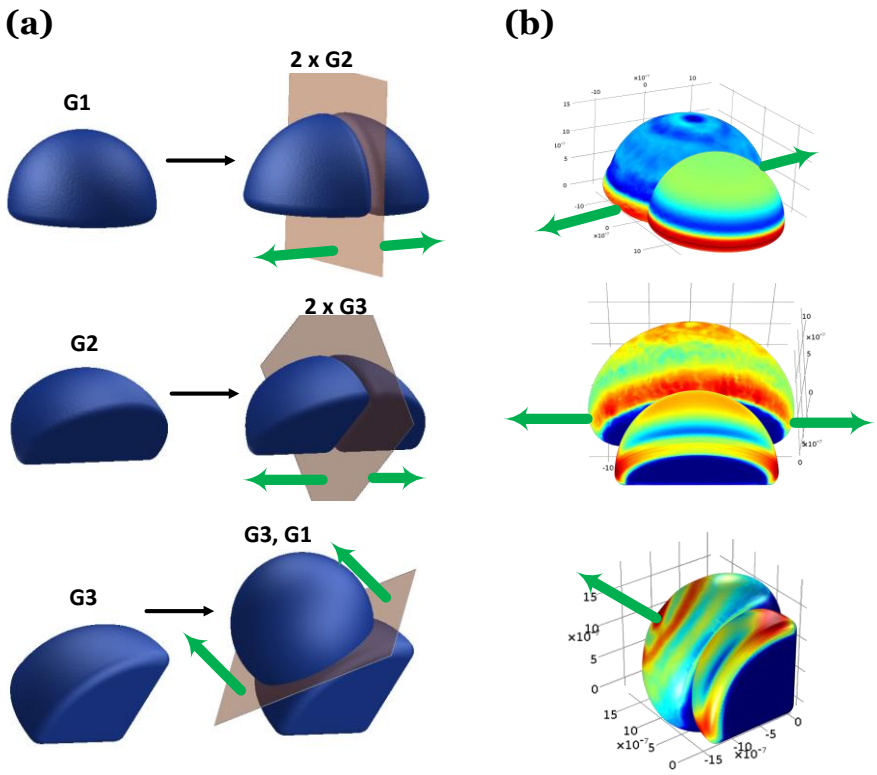

Fig. S2. Principal growth directions in spatially confined cells.
Pink planes indicate a prospective division planes. Green arrows indicate principal growth directions. Black arrow indicates cells transformations due to growth. **(a)** Cell in conformation G1 stretching during growth and transforms to two cells in conformation G2. Cell in conformation G2 stretching during growth (in another direction) and transforms to two cells in conformation G3. This last geometry can either transform to weakly confined spherical cell - which constitutes the complete tetrad morphology; or transforms to a new conformation G1 - that constitutes the initiation of pseudoparenchyma morphology. (b) The results of simulated growth. The graphs show cells geometries at the initial moment of time and when cells volume is doubled. The arrows indicate principal growth directions.

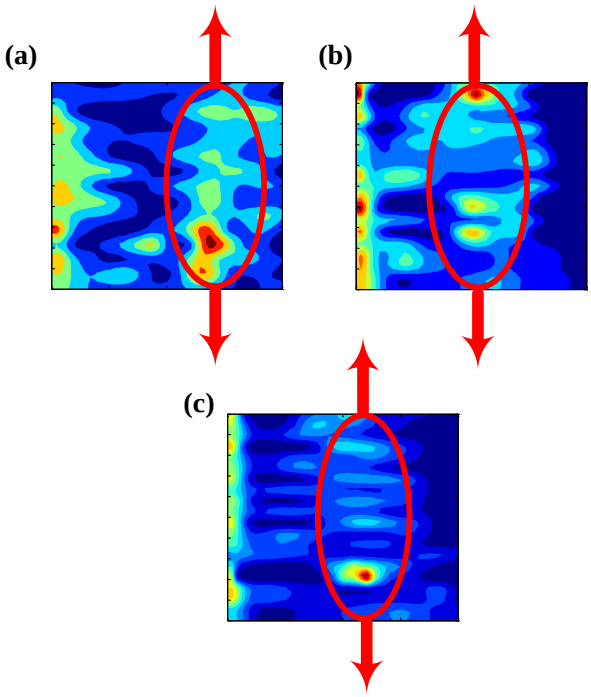

Fig. S3. Anisotropy in growth potential density distribution preserves the principal growth directions observed on anisotropy maps. **(a)** Anisotropy map for G1 conformation, **(b)** for G2 conformation, **(c)** for G3 conformation.

6. Calculations flow scheme of growth problem

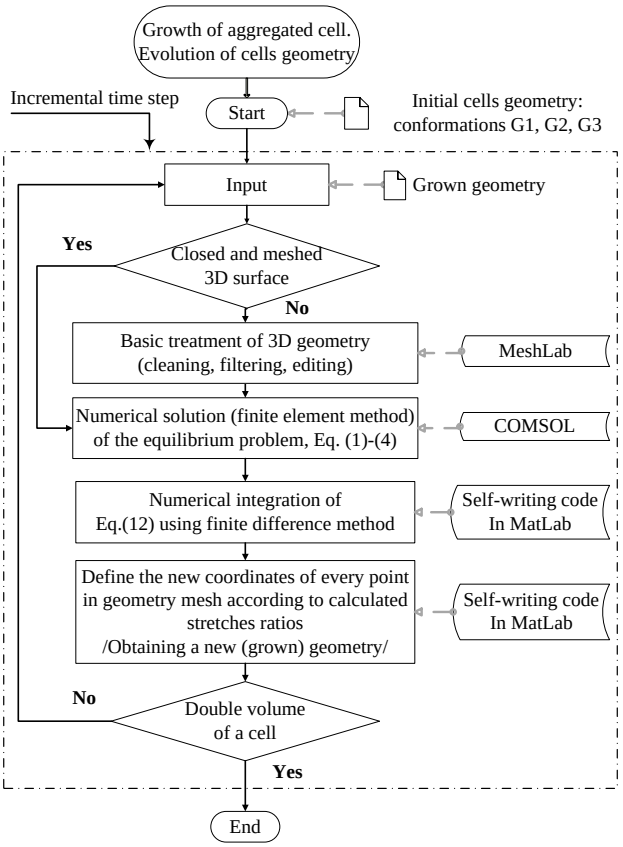

Fig. S4. Calculations flow scheme of growth problem.

Each incremental time step consists of following stages: 1) the problem starts with an initial geometry which is one of three representative conformations (Fig. 5); next 2) we mesh the geometry (using MeshLab v. 1.3.2.) and 3) start solving the equilibrium problem, Eq. (1)-(4), (using COMSOL Multiphysics 4.3a) which gives the stress field for confined shell; then 4) solve Eq. (12) which gives the growth induced strain field and the necessary stretches ratios (using a self-writing code in MatLab R2010b); next stage is 5) performing the necessary cells geometry changes using calculated stretches ratios (using a self-writing code in MatLab R2010b); after which 6) we check whether a cells volume is doubled, if yes – the calculations is stopped, otherwise the new incremental time step is initiated, the new (modified) geometry is used as an input.

References

1. S.-V. Albers and B. H. Meyer, *Nature Reviews Microbiology*, 2011, **9**, 414-426.
2. A. Gambacorta, A. Gliozzi and M. Derosa, *World Journal of Microbiology & Biotechnology*, 1995, **11**, 115-131.
3. G. D. Sprott, C. J. Dicaire, C. G. Choquet, G. B. Patel and I. Ekiel, *Applied and Environmental Microbiology*, 1993, **59**, 912-914.
4. M. A. Arbing, S. Chan, A. Shin, T. Phan, C. J. Ahn, L. Rohlin and R. P. Gunsalus, *Proceedings of the National Academy of Sciences of the United States of America*, 2012, **109**, 11812-11817.
5. R. W. Robinson, *Applied and Environmental Microbiology*, 1986, **52**, 17-27.
6. K. R. Sowers, J. E. Boone and R. P. Gunsalus, *Applied and Environmental Microbiology*, 1993, **59**, 3832-3839.
7. G. Seltmann and O. Holst, *The Bacterial Cell Wall*, Springer, 2002.
8. H. C. Aldrich, R. W. Robinson and D. S. Williams, *Systematic and Applied Microbiology*, 1986, **7**, 314-319.
9. P. Kreisl and O. Kandler, *Systematic and Applied Microbiology*, 1986, **7**, 293-299.
10. M. A. Rodriguez-Carvajal, A. Imberty and S. Perez, *Biopolymers*, 2003, **69**, 15-28.
11. J. E. Scott, Y. Chen and A. Brass, *European Journal of Biochemistry*, 1992, **209**, 675-680.
12. B. M. Sattelle, J. Shakeri, I. S. Roberts and A. Almond, *Carbohydrate Research*, 2010, **345**, 291-302.
13. D. Ambrosi and F. Guana, *Mathematics and Mechanics of Solids*, 2007, **12**, 319-342.
14. D. Ambrosi and A. Guillou, *Continuum Mech. Thermodyn.*, 2007, **19**, 245-251.
15. J. W. C. Dunlop, F. D. Fischer, E. Gamsjaeger and P. Fratzl, *Journal of the Mechanics and Physics of Solids*, 2010, **58**, 1073-1087.
16. T. Bleha and P. Cifra, *Polymer*, 2003, **44**, 3745-3752.
17. M. Dijkstra, D. Frenkel and H. N. W. Lekkerkerker, *Physica A*, 1993, **193**, 374-393.
18. T. W. Burkhardt, *Journal of Physics a-Mathematical and General*, 1995, **28**, L629-L635.
19. Y. Yang, T. W. Burkhardt and G. Gompper, *Physical Review E*, 2007, **76**.
20. A. Menzel and E. Kuhl, *Mechanics Research Communications*, 2012, **42**, 1-14.
21. H. Altenbach, V. A. Eremeev and N. F. Morozov, *Mech. Sol.*, 2010, **45**, 331-342.
22. D. J. Steigmann, *Journal of Elasticity*, 2013, **111**, 91-107.
23. A. F. Bower, *Applied Mechanics of Solids*, Taylor & Francis, 2011.
24. W. B. Whitman, T. L. Bowen and D. R. Boone, *The Methanogenic Bacteria*, 2006.
25. Y. Liu and W. B. Whitman, in *Incredible Anaerobes: From Physiology to Genomics to Fuels*, ed. J. M. R. J. A. M. W. W. Wiegel, 2008, vol. 1125, pp. 171-189.
26. M. M. Kendall and D. R. Boone, *The Order Methanosarcinales*, 2006.
27. P. C. Bressloff and J. M. Newby, *Reviews of Modern Physics*, 2013, **85**, 135-196.
28. D. Chowdhury, *Physics Reports-Review Section of Physics Letters*, 2013, **529**, 1-197.
29. Q. Hong, *Journal of Statistical Physics*, 2010, **141**, 990-1013.
30. D. Huh and J. Paulsson, *Proceedings of the National Academy of Sciences of the United States of America*, 2011, **108**, 15004-15009.
31. S. Sengupta, J. Derr, A. Sain and A. D. Rutenberg, *Physical Biology*, 2012, **9**.
32. P. Borowski and E. N. Cytrynbaum, *Physical Review E*, 2009, **80**.
33. L. I. Rothfield and C. R. Zhao, *Cell*, 1996, **84**, 183-186.
34. C. Jacobs and L. Shapiro, *Proceedings of the National Academy of Sciences of the United States of America*, 1999, **96**, 5891-5893.
35. I. Barak and A. J. Wilkinson, *Fems Microbiology Reviews*, 2007, **31**, 311-326.
36. M. Almonacid and A. Paoletti, *Seminars in Cell & Developmental Biology*, 2010, **21**, 874-880.
37. M. G. Pinho, M. Kjos and J.-W. Veening, *Nature Reviews Microbiology*, 2013, **11**, 601-614.